

CM<sup>2</sup>



# MAGAZINE

第 22 期



南方科技大学海洋磁学中心主编

## 创刊词

海洋是生命的摇篮，是文明的纽带。地球上最早的生命诞生于海洋，海洋里的生命最终进化成了人类，人类的文化融合又通过海洋得以实现。人因海而兴。

人类对海洋的探索从未停止。从远古时代美丽的神话传说，到麦哲伦的全球航行，再到现代对大洋的科学钻探计划，海洋逐渐从人类敬畏崇拜幻想的精神寄托演变成可以开发利用与科学的研究的客观存在。其中，上个世纪与太空探索同步发展的大洋科学钻探计划将人类对海洋的认知推向了崭新的纬度：深海 (deep sea) 与深时 (deep time)。大洋钻探计划让人类知道，奔流不息的大海之下，埋藏的却是亿万年的地球历史。它们记录了地球板块的运动，从而使板块构造学说得到证实；它们记录了地球环境的演变，从而让古海洋学方兴未艾。

在探索海洋的悠久历史中，从大航海时代的导航，到大洋钻探计划中不可或缺的磁性地层学，磁学发挥了不可替代的作用。这不是偶然，因为从微观到宏观，磁性是最基本的物理属性之一，可以说，万物皆有磁性。基于课题组的学科背景和对海洋的理解，我们对海洋的探索以磁学为主要手段，海洋磁学中心因此而生。

海洋磁学中心，简称  $CM^2$ ，一为其全名“Centre for Marine Magnetism”的缩写，另者恰与爱因斯坦著名的质能方程  $E = MC^2$  对称，借以表达我们对科学巨匠的敬仰和对科学的不懈追求。

然而科学从来不是单打独斗的产物。我们以磁学为研究海洋的主攻利器，但绝不仅限于磁学。凡与磁学相关的领域均是我们关注的重点。为了跟踪反映国内外地球科学特别是与磁学有关的地球科学领域的最新研究进展，海洋磁学中心特地主办  $CM^2$  Magazine，以期与各位地球科学工作者相互交流学习、合作共进！

“海洋孕育了生命，联通了世界，促进了发展”。21 世纪是海洋科学的时代，由陆向海，让我们携手迈进中国海洋科学的黄金时代

# 目 录

研究进展 .....	1
QSR: 上-更新世以来南海深层水与陆源输入响应机制 .....	1
海磁文苑 .....	6
对科研的理解 .....	6
岩石磁学演绎 .....	7
第 12 章 磁滞回线—SP 与 MD 颗粒 .....	7
文献导读 .....	11
1. 晚白垩纪太平洋底层水来源及相对流速的制约 .....	11
2. 镁铁质岩浆系统中贵金属矿化层的快速结晶 .....	14
3. MIS 11 初期异常高的生物圈生产力 .....	16
4. 新的磁测资料显示南海在海底扩张过程中出现了连续的洋脊跃迁 和旋转 .....	19
5. 海底磁化强度: 低温氧化导致的钛磁铁矿颗粒的压力和结构变化 .....	22
6. 根据新的重力(EIGEN 6C4)及其他方面数据确定在西伯利亚 (Popigai)附近的一个 200km 疑似陨石坑 Kotuykanskaya .....	24
7. 葫芦洞石笋记录的末次冰期大气 $^{14}\text{C}/^{12}\text{C}$ 变化 .....	26
8. 南海中新世晚期 <i>Tridacnidae</i> 碳同位素变化的控制机制 .....	28
9. 温度和海水同位素组成对日本沿海两根 83ka 以来的石笋记录的控 制 .....	30

## 研究进展

### QSR: 上-更新世以来南海深层水与陆源输入响应机制

早更新世在东亚地区乃至全球气候系统都发生明显的变化，表现在大气环流和洋流体系两个方面，尤其是北极冰盖的扩张和亚洲内陆干旱化。全球气候系统经历了两个重要转型期：上新世转型(late Pliocene transition, LPT)和中更新世的转型(mid-Pleistocene transition, MPT)。前人认为碳循环、冰盖的扩张、构造抬升以及海道的关闭都是气候转型的主要因素。然而，对于上新世以来大气环流和深水洋流系统的控制机制存在争议。

北太平洋地区是大洋环流传输的终端，也是全球碳储库之一。因此，理解太平洋深层水的变化对于探索海洋对于全球碳排放和营养盐的重要调控作用十分重要(图1)。南海作为西太平洋最大的半封闭边缘海，吕宋海峡是沟通太平洋与南海的唯一通道，因此南海海洋环流变化响应于太平洋深层水变化(图2)。另外，大陆的风化输入进入南海，南海较高的沉积速率也可以很好地响应气候变化特征。前人研究往往只从南海的某一角度出发，探讨其环流环境和陆源输入模式，而对于二者如何响应全球气候转型变化还存在争议。

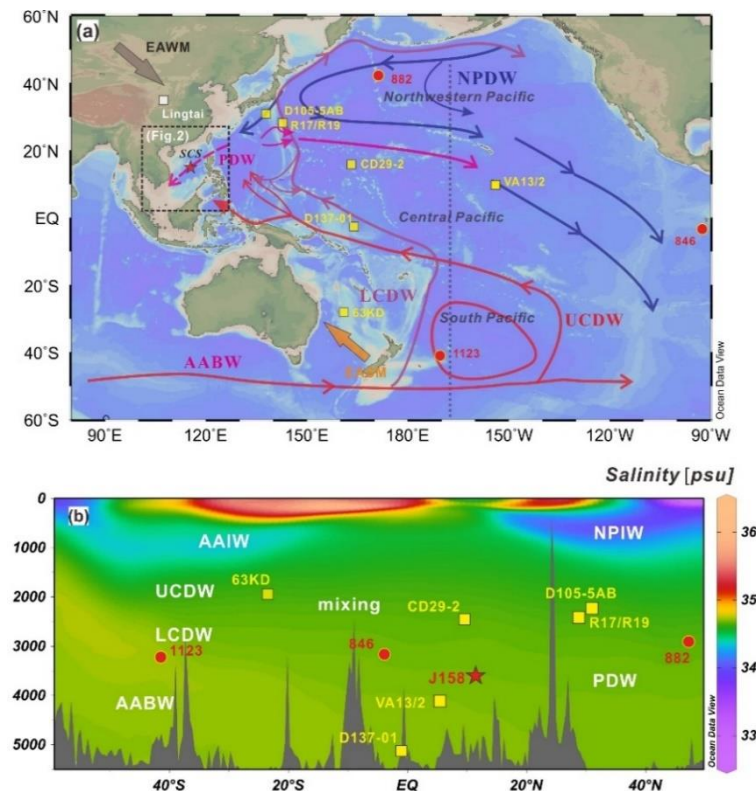


图1. 研究站位及全球水团分布特征

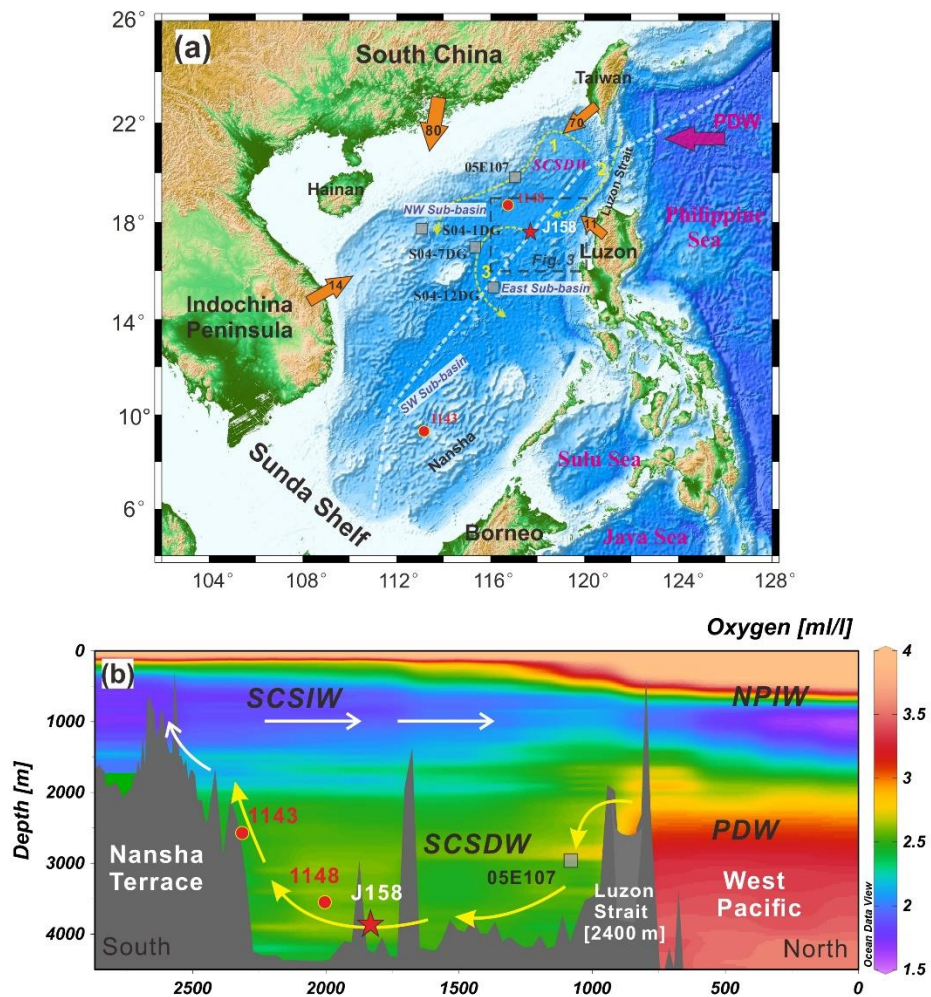


图 2. 研究区域沉积与洋流环境。红色圆点和黄色方块分别代表前人研究的南海海洋沉积物岩芯和多金属结核、结壳（沉积物包括 ODP 1143 和 ODP1148；多金属结核、结壳包括 05E107, S04-1DG, S04-7DG 和 S04-12DG）粉色箭头是深层水：1. 南海等深流；2.吕宋深水洋流；3. 深部气旋环流。

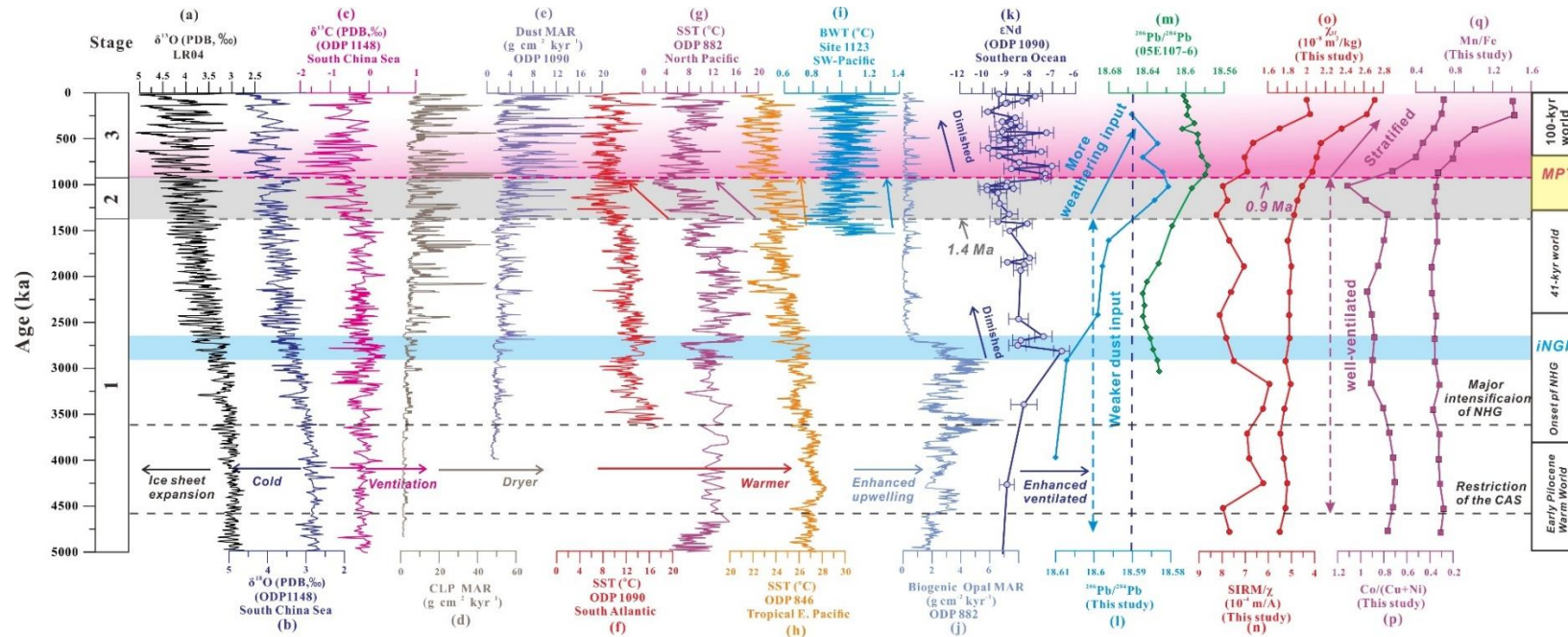


图 3. J158 站位的 Pb 同位素、地球化学和磁学结果及其他风尘堆积速率和海洋与陆地的记录。(a) ODP 1148 站位的底栖有孔虫  $\delta^{18}\text{O}$  记录; (b) ODP 1148 站位的底栖有孔虫的  $\delta^{13}\text{C}$  记录; (c) 中国黄土堆积速率; (d) 北太平洋 ODP 882 的海表温度 (SST); (e) 赤道东太平洋 ODP 846 站位的海表温度 (SST); (f) 西南太平洋 ODP 1123 的底层水温度 (BWT) 记录; (g) 北太平洋 ODP 882 站位生物蛋白石通量; (h) 南海 05107-6 结核  $^{206}\text{Pb}/^{204}\text{Pb}$  记录; (i) 南海 J158 结核  $^{206}\text{Pb}/^{204}\text{Pb}$  记录; (j) J158 结核的低频磁化率 ( $\chi$ ) 记录; (k) 结核 J158 站位 SIRM/ $\chi$  记录; (l) 结核 J158 的 Mn/Fe 比值记录; (m) 结核 J158 的 Co/(Cu + Ni) 比值记录

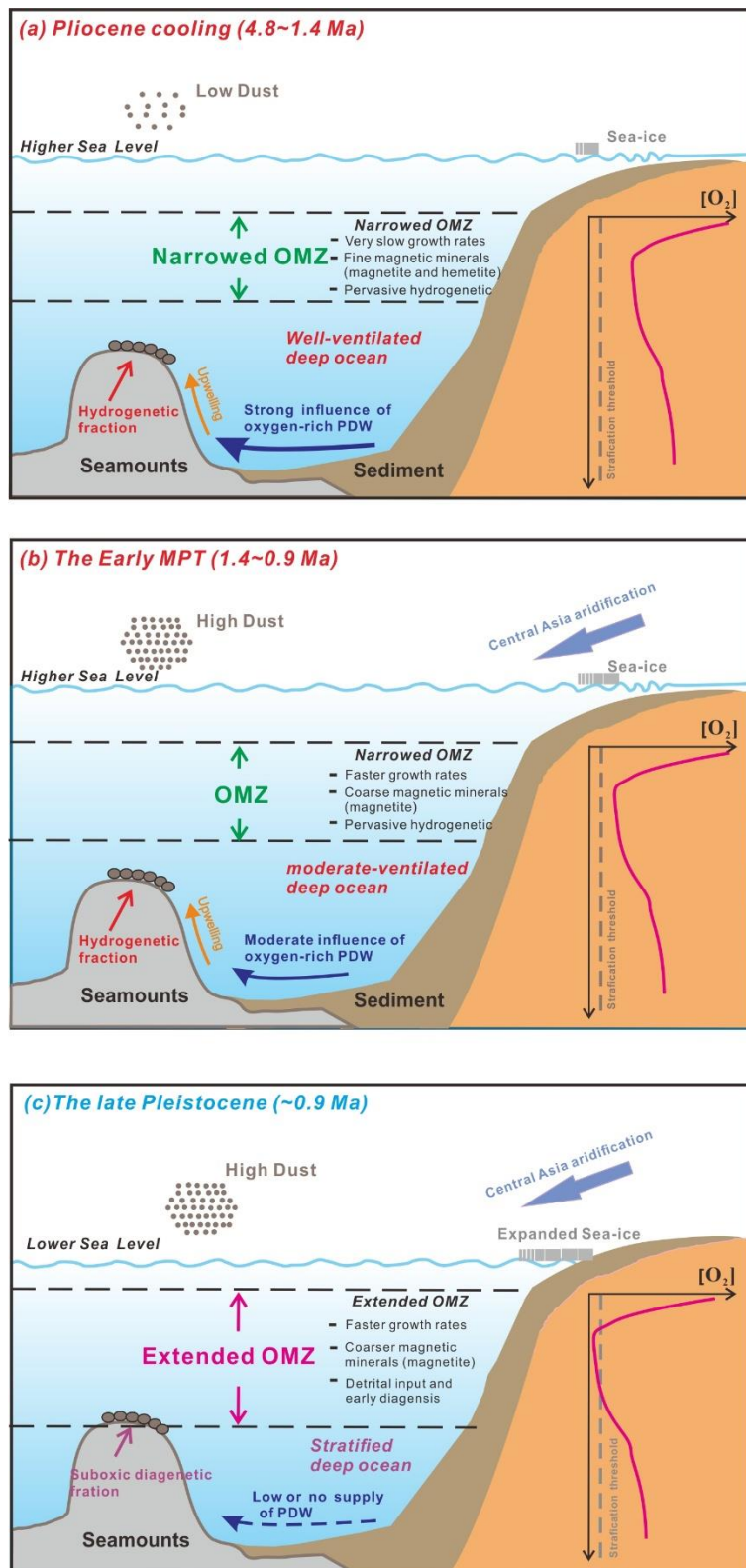


图 4. 4.8 Ma 以来南海海洋和陆源环境变化 (a) 上新世变冷时期，南海深水环境表现为深层通风作用增强，亚洲风尘降低为特征；(b) 早中更新世早期，南海深部表现为中度氧化富集深层水和由于东亚干旱化加强导致的风尘逐步增强有关；(c) 在中更新世晚期，南海深部表现为太平洋深层输入降低，亚洲内陆干旱化降低。

南海多金属结核尤以铁锰氧化物为主，沉积速率较慢，既可以记录周边海水环境的特征，也可以反映百万年尺度上的陆源输入的变化（Zhong et al., 2019）。

基于南海多金属结核地球化学、岩石磁学变化及 Pb 同位素物源变化特征，将南海过去 4.8 Ma 的古海洋变化分为三个阶段：阶段 1：~4.8-1.4 Ma，阶段 2：1.4-0.9 Ma，阶段 3：~0.9 Ma。阶段 1 时期 (~4.8-1.4 Ma)，南海深水环境表现为深层通风作用增强，亚洲风尘降低的特征；阶段 2 (1.4-0.9 Ma)，南海深部表现为中度氧化富集深层水和由于东亚干旱化加强导致的风尘逐步增强有关；阶段 3 (~0.9 Ma)，南海深部表现为太平洋深层水输入降低，全球变冷导致亚洲内陆干旱化进一步加强（图 3）。

我们的结果发现在气候过渡阶段时期，全球变冷是北半球高纬度海洋内部分层、大气环流和风尘通量输入的主要驱动力。然而，北半球高纬度永久性分层作用无法影响南海深水环境。而且，南海深水环流和陆源风化输入的不一致性特征可能与中更新世转型期冰期转化的临界点有关（图 4）。

#### 相关文献：

**Yi Zhong**, Qingsong Liu, Zhong Chen\*, et al. Tectonic and paleoceanographic conditions during the formation of ferromanganese nodules from the northern South China Sea based on the high-resolution geochemistry, mineralogy and isotopes, *Marine Geology*, 2019, 410, 146~163.

**Yi Zhong**, Zhong Chen, Qingsong Liu\*, et al., Evolution of a deep-water ferromanganese nodule in the South China Sea in response to Pacific deep-water circulation and continental weathering during the Plio-Pleistocene, *Quaternary Science Reviews*, 2020, 229, 106106. <https://doi.org/10.1016/j.quascirev.2019.106106>.

## 对科研的理解

郑威

简而言之，科研是人类对未知事物不断探索的一个过程，从一个假设开始出发，获取需要的数据，从数据中提取信息，从信息中获取知识，并且合理地去解释，理解这些知识。再理解了新知识后，可能还会有新的思路涌现，那么又开始重新获取新的数据-信息-知识-新的理解。科研，就是重复这些步骤，不断获得新的理解。

以我的研究为例，要想探讨气候环境变化对古人类活动的影响，那么就需要去古人类活动区域获取能够记录古气候古环境信息的载体，所以我们采集了古人类活动洞穴遗址的石笋样品，依靠 U-Th 定年、<sup>14</sup>C 定年获取石笋的年代框架，及碳屑层的年代，测环境磁学、氧碳同位素等参数，获取原始数据，得到数据高低变化的信息，结合年代，我们可以推测这些数据的高低变化代表何种的气候环境变化，并且用合理的故事来理解与解释这些变化与古人类活动行为之间的联系。在我们理解这些知识，并作出解释的时候，可能还会发现一些存疑的地方，那么我们就需要针对这些地方做出假设，并获取新的数据来验证我们的假设。

以上，是技术性层面对科研的理解，科研同样也是一门社会学。

科研不是一个人的工作，需要各方面的协调与配合，不仅有组内的合作交流，也需要与很多合作者，以及校内外的部门，人员打交道。在组内，需要人员协调实验仪器最优化使用，当组内仪器不能满足实验要求时，还需要寻找合适的单位协商借用仪器。对于出野外的安排，需要与当地主管部门协商，与所有合作者规划行程等。在这些事情中就隐藏着很多复杂的社会关系，如何与人打好交道，也成了科研中的重要一环。

## 岩石磁学演绎

### 第 12 章 磁滞回线—SP 与 MD 颗粒

由于热能足够大，SD 颗粒能够克服能垒，其 M 可自由偏转，从而变为 SP 状态，其矫顽力和剩磁矫顽力均为零。

其归一化 M-H 曲线服从朗之万方程：

$$M(H_0, T) = M_s L(\alpha) = M_s [\coth(\alpha) - 1/\alpha],$$

其中  $\alpha = \mu_0 V M_s H / kT$ 。

当外场很小时， $L(\alpha) = \alpha/3$ ，于是

$$M = \mu_0 V M_s^2 H / 3kT$$

可见对于 SP 颗粒的初始磁化率为：

$$dM/dH = \mu_0 V M_s^2 / 3kT$$

对于单一粒径的 SP 颗粒，随着温度升高，其磁化率值降低。当 SP 颗粒的粒径增大时，SP 颗粒的磁化率和其体积成正比。因此，粒径比较大的 SP 颗粒其磁化率对样品的磁化率贡献最大。对于很小的 SP 颗粒(比如几个纳米)，在室温，即使存在于样品中，其对磁化率的贡献也很小。只有降低温度，其作用才能逐渐凸显。因此，低温(<300 K)技术能有效地检测小粒径 SP 颗粒。

因为 SP 颗粒的磁化率曲线服从朗之万方程，所以把 SD 颗粒解阻后，测量它的磁滞回线，通过拟合朗之万方程，就可以获得 SP/SD 颗粒的体积。

我们需要注意到，SP 和顺磁颗粒的区别在于，SP 颗粒的 M-H 曲线符合朗之万方程，和 SD 一样，M 能够被饱和。而顺磁颗粒的 M-H 曲线就是一条过原点的直线。

现在我们再考察一下 MD 颗粒的磁滞回线。MD 颗粒的矫顽力很小，这就暗

示着它的磁滞回线非常狭窄，但是绝对不是 SP 颗粒那样矫顽力为零。

MD 颗粒与 SP 颗粒具有外形相似的磁滞回线，但是其机制完全不同。SP 颗粒的矫顽力为零，也就是说其正向场和反向场的磁滞回线完全重合。MD 颗粒的正向和反向磁滞回线不重合，具有较小的矫顽力。对于大颗粒 MD 磁铁矿，其矫顽力一般小于十几个 mT。

与 SD 颗粒不同，MD 颗粒主要通过磁畴壁的移动来改变其磁化状态。以两磁畴颗粒为例，在无外场的均衡状态下，两个磁畴体积相等，磁化方向刚好相反，整体磁化强度为零。当加入外场时，磁畴壁会移动，磁化强度方向与外场方向相同的磁畴体积增大，从而整体上磁化强度增加。

如果样品中的磁畴变化不大，比如， $M_{rs}$  和  $M_s$  完美地线性相关，那么  $M_{rs}$  和  $M_s$  都可以用来表示磁性矿物含量的变化。

多畴颗粒内部经常含有晶格缺陷、空位、微小楔入体等，就类似于我们行军路上碰到的沟沟坎坎，从而对磁畴壁有一定的阻挡作用，这种局部的阻挡力称之为  $h_c$ 。只有当外场克服  $h_c$  时，磁畴壁才能继续向前运动，直到遇到新的阻挡力。因此，多畴颗粒的磁滞回线在微观上并不平滑，而是具有阶梯状的特征，磁畴壁每一次跳跃，称之为巴尔克豪森(Barkhausen)跳跃。

如果我们把 MD 颗粒的 M-H 曲线局部放大，就会发现 M 并不是连续变化，而是像台阶那样一节一节地跳跃。这就是磁畴壁克服局部  $h_c$  的现象。早期物理学家没有设备来真正看到这种微观结构上的变化，但是他们想到了一个绝佳的方案，把 M 这种跳跃式的变化转换成电流，然后再转化成声音高低的变化。于是，我们在磁化过程中，就会听到噼噼啪啪的声音，可以断定 M 是阶梯式变化，而不是连续变化。

在磁畴壁偏离平衡位置向右移动的过程中，外场越大，磁畴壁会克服更高的 $h_c$ ，从而偏离平衡位置越远。去除外场后，在退磁场的作用下，磁畴壁向左朝初始的平衡位置移动，在返回的路径过程中，会被之前遇到的沟坎阻挡住，从而获得一个较小的剩磁。SD 颗粒改变磁化状态需要旋转其磁化轴，因而具有较高的矫顽力( $> 20$  mT)。对 MD 颗粒而言，由于阻挡磁畴壁移动而造成的矫顽力值远小于 20 mT。

我们可以预计，外场越大，磁畴壁移动的路程越远，去除外场后，越可能被更大的沟沟坎坎拦截住，所以会停留在离平衡状态更远的地方，从而获得更大的剩磁。

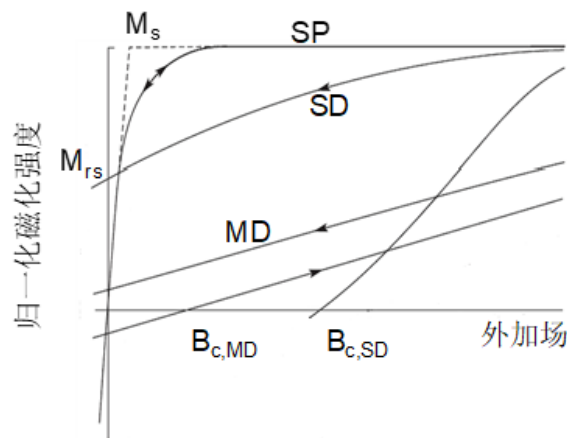


图 1 SP、SD、和 MD 颗粒部分磁滞回线对比图。

通过图 1，我们对比了 SP、SD、MD 在第一象限内的磁滞回线。对于磁铁矿，无论其处于任何磁畴状态，它们的饱和磁化强度都是一样。在饱和状态下，所有的磁矩都像一把筷子一样指向一个方向。当去除外场后，这些磁矩就像孔雀开屏，或者打开一把扇子一样在半平面打开，于是通过积分我们就可以得到，SD 颗粒的饱和剩磁  $M_{rs}$  只有  $M_s$  的一半。SP 颗粒没有剩磁。MD 颗粒虽然有剩磁，但是和 SD 的剩磁比起来，就小得多。

自然界样品中含有很多颗粒，为了去除含量的影响，我们通常可以用  $M_{rs}/M_s$

来衡量磁畴的变化。如果这个比值接近 0.5，说明应该是拉长型的 SD 颗粒占主导。不过，如果这个比值很低，就会出现多解性。这既可以对应着 SP 颗粒含量高，也可以对应着 MD 颗粒含量高。

在文献中，我们会遇到两种饱和等温剩磁。第一种就是我们通过磁滞回线得到的  $M_{rs}$ 。第二种的获得方式更直接，用一个强磁场，或者一个磁铁，直接把样品磁化，获得的剩磁就是饱和等温剩磁（Saturation Isothermal Remanent Magnetization, SIRM）。

如果把  $M_{rs}$  和 SIRM 做线性相关图，一定会线性相关，但是一般情况下 SIRM 一定会比  $M_{rs}$  要低。

这两种饱和等温剩磁的区别在哪里？

答案是获得方式不同。前者是测量磁滞回线的副产品，在同一台仪器上获得。SIRM 则是先磁化，然后放到 JR6 或者超导磁力仪上去测得到的结果。对于单独一块样品，后者所需要的实验时间要比前者多。

我们知道剩磁的携带者中含有 VSP 成分。VSP 携带的剩磁会随着时间衰减。时间越长，衰减得越多。所以在测 SIRM 时，尤其是测量一批样品时，我们常常是先把样品整体磁化，然后再一个一个测量，需要时间较长，所以 VSP 颗粒的剩磁就会较为充分地衰减，SIRM 整体值就会偏低。VSM 测量磁滞回线所需时间整体偏短，所以  $M_{rs}$  就会高一些。

事实上，如果用 VSM 把样品饱和磁化，然后测量其  $M_{rs}$  随时间的变化，就会得到一条  $M_{rs}$  随时间的衰减曲线。我们通过  $M_{rs}(t)$  的衰减行为就可以得出样品中 VSP 含量的相对变化。可以进一步肯定的是， $M_{rs}$  的衰减量会和样品的绝对频率磁化率值正相关，因为它们都是衡量 VSP 颗粒含量的参数。

## 文献导读

### 1. 晚白垩纪太平洋底层水来源及相对流速的制约



翻译人：仲义 zhongy@ustech.edu.cn

Shannon J. Haynes, Kenneth G. MacLeod, Jean-Baptiste Ladant, et al., **Constraining sources and relative flow rates of bottom waters in the Late Cretaceous Pacific Ocean [J]**, *Geology*, 2020, 48: 509-513. Doi: 10.1130/g47197.1

**摘要：**地球化学结果显示在白垩纪最后 10 百万年间（晚坎帕阶-麦斯里希特阶）海洋环流模式发生转变。前人认为南大西洋和印度洋的深水形成和增强是北大西洋深层水的开端和引擎，并进一步改变北太平洋和南太平洋区域性的深层水翻转作用。现存的地球化学数据无法简单支持或者反对这种情况，为了验证麦斯里希特阶的太平洋环流，利用麦斯里希特阶古地理和前人研究结果，我们利用四根中太平洋海山区和沙茨基隆起区岩心的 Nd 同位素数据，以及地球系统模型结果，发现在麦斯里希特阶变冷早期（EMCP）存在~1-3 百万年的 Nd 同位素负漂移，但是在晚坎帕阶-晚麦斯里希特阶 (~10 百万年间) 没有其他持续变化的趋势。模拟结果显示不同的二氧化碳营力导致循环速率的变化，而非洋流循环模式控制。这些结果共同支持在晚坎帕阶-晚麦斯里希特阶阶段，西南太平洋地区具有持续性的中-深层水的输入，而 EMCP 时期 Nd 同位素变化的原因是由于太平洋洋流翻转的速率加剧导致的，而非太平洋底层水来源的变化。

**ABSTRACT:** Geochemical data suggest that ocean circulation patterns changed over a period of longterm cooling during the last 10 m.y. of the Cretaceous (late Campanian–Maastrichtian). Proposed changes include enhanced deep-water formation in the South Atlantic and/or Indian sectors of the Southern Ocean, initiation or enhanced deep-water formation in the North Atlantic, and alternating regions of deep convection in the North and South Pacific. Existing geochemical data do not allow simple confirmation or rejection of any of these scenarios. To test Pacific circulation during the Maastrichtian, we measured neodymium isotopic ( $\epsilon_{Nd}$ ) values from four Pacific Deep-Sea Drilling Project and Ocean Drilling Program sites and compare results both to Earth system model simulations using Maastrichtian paleogeography and to previous studies.

Pacific  $\epsilon_{\text{Nd}}$  results consistently show a small negative  $\epsilon_{\text{Nd}}$  excursion during a well-documented,  $\sim 1$ – $3$  m.y. early Maastrichtian cooling pulse (EMCP) but no other consistent trends across the late Campanian–late Maastrichtian interval ( $\sim 10$  m.y.). Model results show that different CO<sub>2</sub> forcings lead to changes in rates, but not patterns, of circulation. These combined results support the existence of a sustained source region for intermediate and deep waters in the southwestern Pacific throughout the late Campanian–Maastrichtian and indicate that changes in  $\epsilon_{\text{Nd}}$  values during the EMCP reflect an increased rate of overturning in the Pacific rather than changes in the source area of Pacific bottom waters.

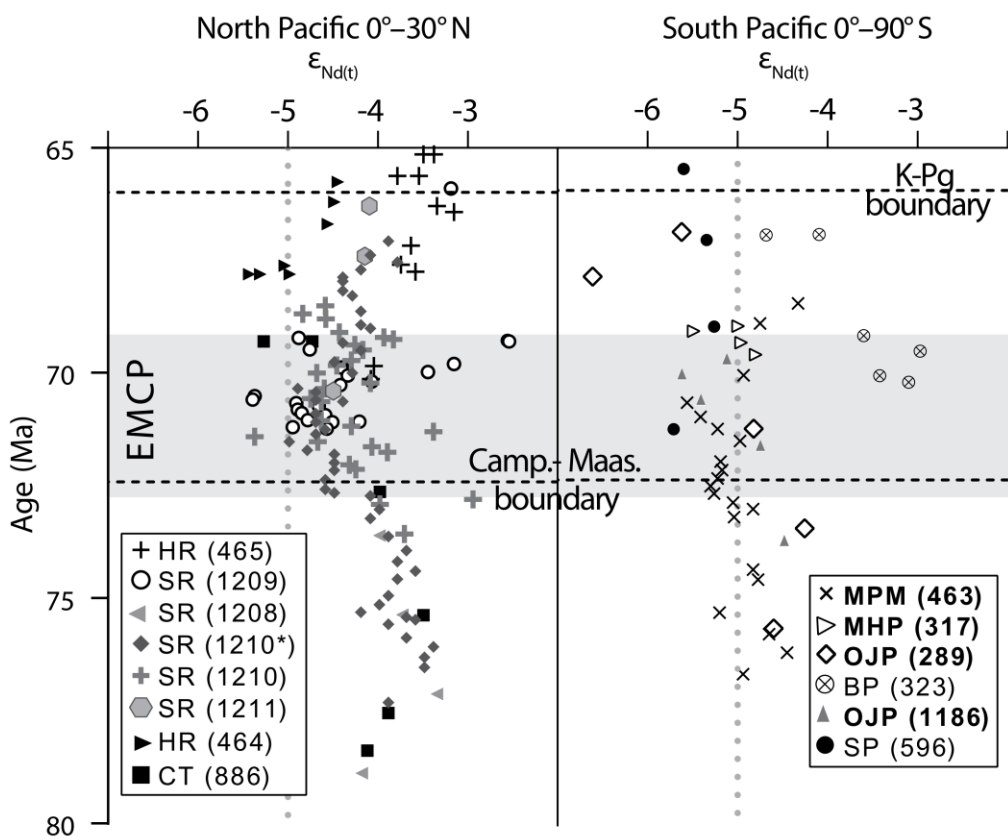


Figure 1. Compilation of new and published Pacific Ocean  $\epsilon_{\text{Nd}}(t)$  data from 80 to 65 Ma. See Figure 1 for location abbreviations. Unless otherwise indicated by an asterisk (for leachates), all Nd was extracted from fish debris. Point markers indicate paleowater depth as follows: line symbols, 0–1.5 km; shapes with no infill, 1.6–2.5 km; gray infill, 2.6–3.5 km; black infill, >3.5 km. Sources for  $\epsilon_{\text{Nd}}(t)$ : Deep Sea Drilling Project (DSDP) Sites 289, 317, 463, Ocean Drilling Program (ODP) Site 1186—this study (bold); DSDP Site 323—Thomas et al. (2014), Moiroud et al. (2016); DSDP Site 464—Hague et al. (2012); DSDP Site 596—Thomas et al. (2014); ODP Site 886—MacLeod et al. (2008); ODP Site 1208—Hague et al. (2012), Murphy and Thomas (2012); ODP Site 1209—Thomas (2004), Frank et al. (2005); ODP Site 1210—Jung et al. (2013), Frank et al. (2005); ODP Site 1211—Thomas (2004). Ages are consistent with 2012 Geologic Time Scale (Gradstein et al.,

2012). Camp.-Maas.—Campanian-Maastrichtian; EMCP—early Maastrichtian cooling pulse; K-Pg—Cretaceous-Paleogene.

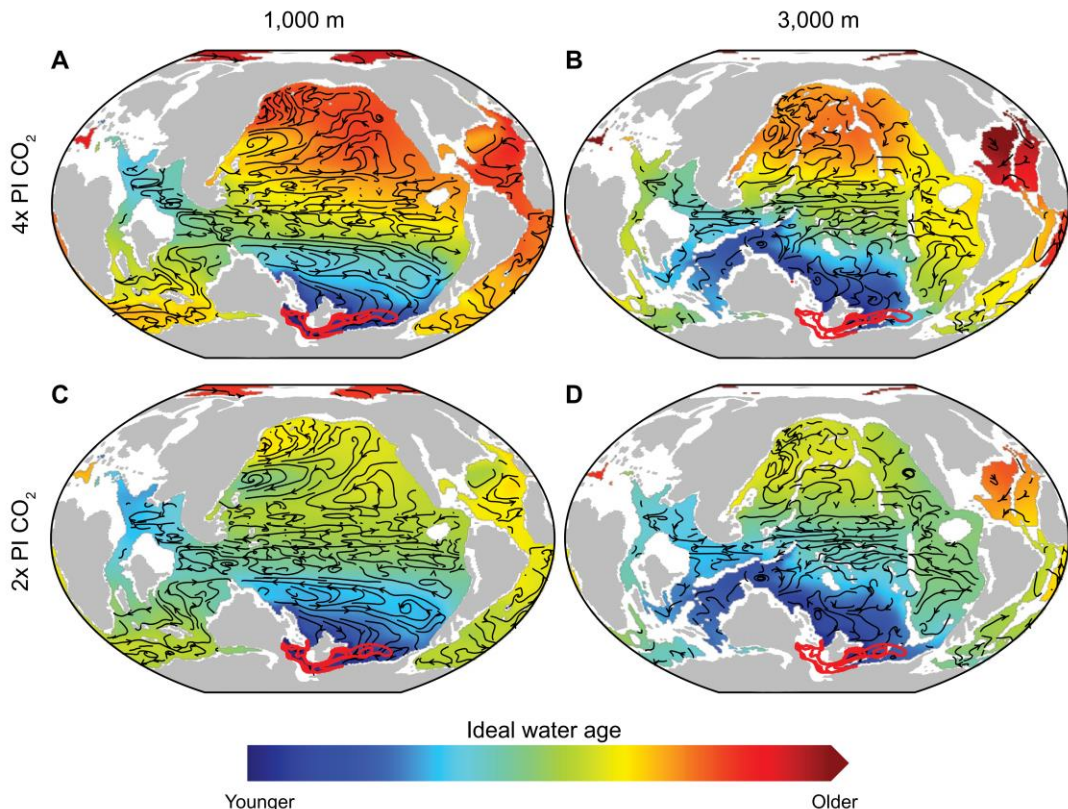


Figure 2. Ocean-climate model simulations of ideal water mass age at 1000 and 3000 m below sea level in the Maastrichtian with 2 $\times$  and 4 $\times$  pre-industrial (PI) CO<sub>2</sub> concentrations (560 and 1120 ppmv, respectively). Continents are shaded in gray; red contours are maximal Southern Hemisphere late winter (September) mixed-layer depth (1000 m conto

## 2. 镁铁质岩浆系统中贵金属矿化层的快速结晶



翻译人: 冯婉仪 fengwy@sustech.edu.cn

Hepworth L N, Daly S J, Gertisser R, et al. *Rapid crystallization of precious-metal mineralized layers in mafic magmatic systems*[J]. *Nature Geoscience*, 2020, doi: 10.1038/s41561-020-0568-3

**摘要:** 镁铁质岩浆系统的固结残余体是地壳中铂族金属最富集的地方。我们对这些侵入体中贵金属矿化的理解是基于岩浆房过程和晶粥固结的传统观点。尽管这些关键金属对现代社会很重要,但是关于控制它们富集的物理和时间因素仍然存在很大的不确定性。在这里,我们对古近系 Rum 层状侵入体(苏格兰西北部)中数厘米厚的富集贵金属层中的斜长石和单斜辉石进行了高精度的 $^{87}\text{Sr}/^{86}\text{Sr}$ 同位素分析。在整个研究区域内,不同的斜长石晶体、单斜辉石与斜长石晶体之间以及斜长石晶体内部均存在同位素不均一性。根据这些观察结果,我们论证了铂族元素矿化是由于多次小体积的反应熔体渗流事件导致的。保存在 10-100  $\mu\text{m}$  尺度下的锶同位素不均一性指示了导致富集贵金属层形成的熔体的冷凝速度每年超过 1  $^{\circ}\text{C}$ , 并且从冷却到扩散终止发生在数十到数百年内。我们的数据强调了晶粥内周期性的溶解-再结晶事件的重要性,并提出了在岩浆冷却和固结期间,重复的自侵入(self-intrusion)过程可能会导致含贵金属的镁铁质岩体的形成。

**ABSTRACT:** The solidified remnants of mafic magmatic systems host the greatest concentrations of platinum-group metals in the Earth's crust. Our understanding of precious-metal mineralization in these intrusive bodies is underpinned by a traditional view of magma chamber processes and crystal mush solidification. However, considerable uncertainty remains regarding the physical and temporal controls on concentrating these critical metals, despite their importance to modern society. We present high-precision  $^{87}\text{Sr}/^{86}\text{Sr}$  analyses of plagioclase and clinopyroxene from within centimetre-thick precious-metal-enriched layers in the Palaeogene open-system Rum layered intrusion (northwest Scotland). Isotopic heterogeneity is present between plagioclase crystals, between clinopyroxene and plagioclase and within plagioclase crystals throughout the studied section. On the basis of these observations, we demonstrate that platinum-group element mineralization formed by repeated small-volume reactive melt percolation events. The preservation

of strontium isotope heterogeneities at 10-100  $\mu\text{m}$  length scales implies cooling of the melts that formed the precious-metal-rich layers occurred at rates greater than 1  $^{\circ}\text{C}$  per year, and cooling to diffusive closure within tens to hundreds of years. Our data highlight the importance of cyclic dissolution–recrystallization events within the crystal mush and raise the prospect that precious-metal-bearing mafic intrusions may form by repeated self-intrusion during cooling and solidification.

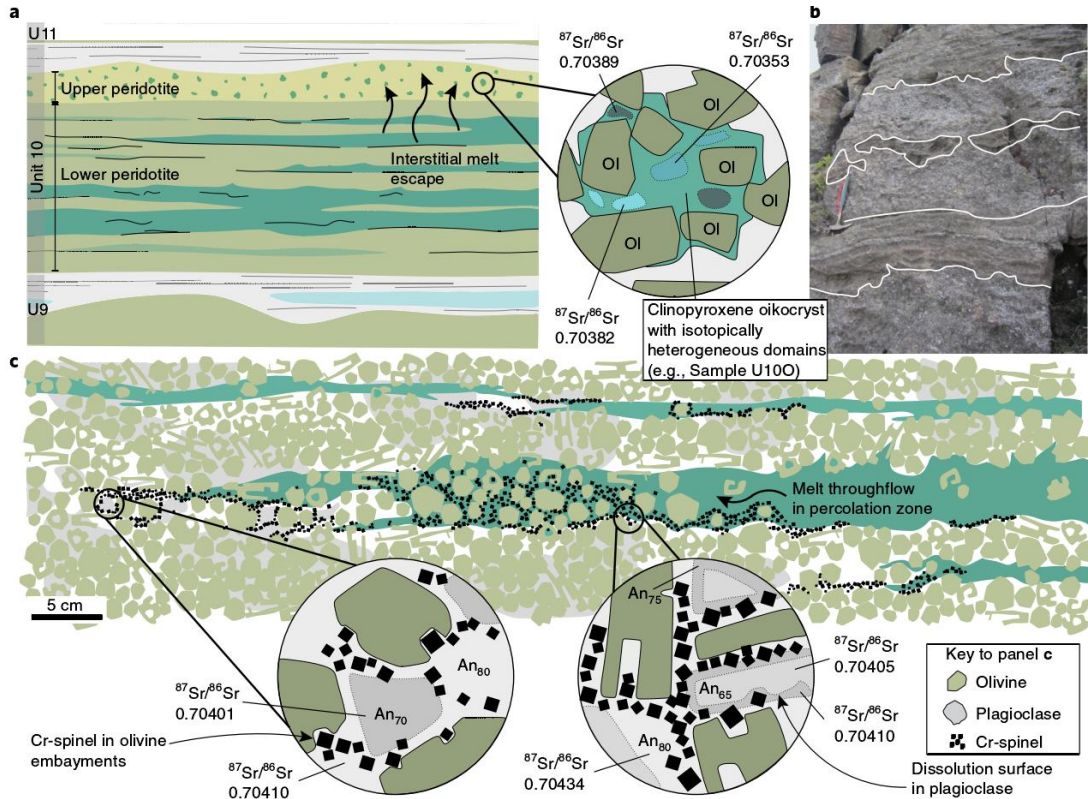


Figure 1. Schematic cartoon illustrating the reactive percolation model discussed in the text. a, The entire Unit 10 sequence. b, Representative field photograph showing typical distributions of intrusive peridotite (highlighted) in outcrop. c, Conceptual illustration (based on the field relationships) of the formation of strontium isotope heterogeneities ( $^{87}\text{Sr}/^{86}\text{Sr}$  values are indicative only) during the formation of one percolation zone (scale is approximate). Note the leading fronts or basal/top contacts of percolation zones (dark green) locally develop chromitite sensu stricto, whereas chain-textured Cr-spinel seams signifying porous reactive flow form around olivine crystals. Reactive percolation zones may locally thin, thicken and bifurcate. The presence of > 100 Cr-spinel seams throughout the Unit 10 lower peridotite implies that numerous percolation zones such as those illustrated in c must have existed. The observation that some Cr-spinel seams bifurcate means that the number of replenishments may be less than the number of Cr-spinel seams, and there is no requirement in our model for ‘stratigraphically’ higher Cr-spinel seams to postdate those that lie underneath them.

### 3. MIS 11 初期异常高的生物圈生产力



翻译人：蒋晓东 jiangxd@sustech.edu.cn

Brandon, M., Landais, A., Duchamp-Alphonse, S., et al. (2020). *Exceptionally high biosphere productivity at the beginning of Marine Isotopic Stage 11*. *Nature Communications*, 11(1), 1-10.

**摘要：**冰期-间冰期循环中大气二氧化碳的显著改变主要归因于南大洋的物理、生物过程。

然而与二氧化碳通量相关的全球生物圈生产力的贡献仍然不清楚。本研究对欧洲南极冰芯计划获取的冰芯进行氧同位素分析，第一次获取了高分辨率的 MIS 11 和冰期终止期 5 以来的  $\Delta^{17}\text{O}$  记录。重建了过去 445 ka 以来全球生物圈的氧气生产力。数据表明，相较于年轻的终止期，晚冰期终止期 5 的生物圈生产力高出 10 - 30%。与先前的观察相比较，在低偏心率的环境下陆地生产力可能解释这一模式。我们认为高的生物圈生产力能够保持 MIS 11 早期较低含量的大气二氧化碳，因而控制冰期终止期 5 的全球气候。

**ABSTRACT:** Significant changes in atmospheric CO<sub>2</sub> over glacial-interglacial cycles have mainly been attributed to the Southern Ocean through physical and biological processes. However, little is known about the contribution of global biosphere productivity, associated with important CO<sub>2</sub> fluxes. Here we present the first high resolution record of  $\Delta^{17}\text{O}$  of O<sub>2</sub> in the Antarctic EPICA Dome C ice core over Termination V and Marine Isotopic Stage (MIS) 11 and reconstruct the global oxygen biosphere productivity over the last 445 ka. Our data show that compared to the younger terminations, biosphere productivity at the end of Termination V is 10 to 30 % higher. Comparisons with local palaeo observations suggest that strong terrestrial productivity in a context of low eccentricity might explain this pattern. We propose that higher biosphere productivity could have maintained low atmospheric CO<sub>2</sub> at the beginning of MIS 11, thus highlighting its control on the global climate during Termination V.

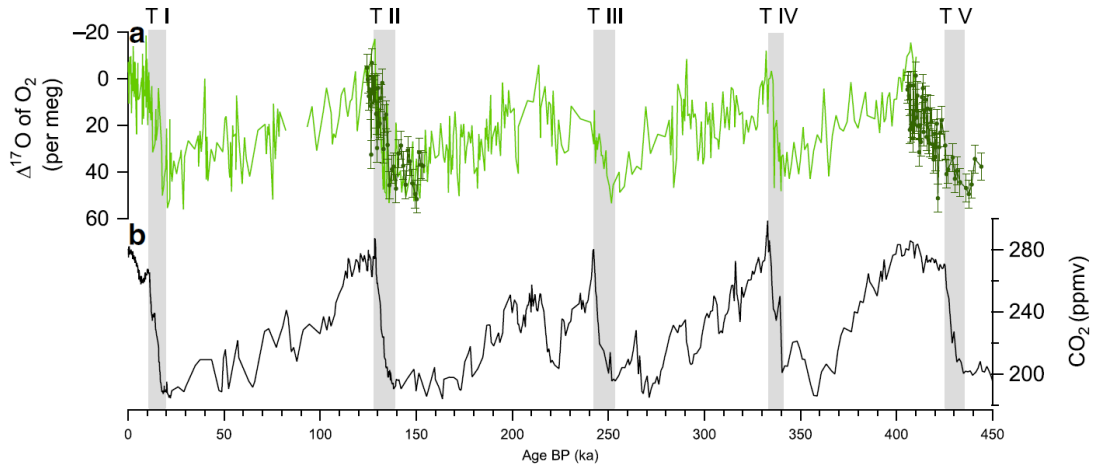


Figure 1. Record of  $\Delta^{17}\text{O}$  of  $\text{O}_2$  over the last 450 ka compared to evolution of  $\text{CO}_2$ . a  $\Delta^{17}\text{O}$  of  $\text{O}_2$  (light green: record presented in Blunier et al. covering the last 400 ka; dark green: new record with error bars showing the standard deviation of  $\pm 6$  per meg). b atmospheric  $\text{CO}_2$  variations over the last 450 ka. The ice core records are presented on the AICC2012 timescale. The grey shadow bars represent the period of rapid increase in atmospheric  $\text{CO}_2$ .

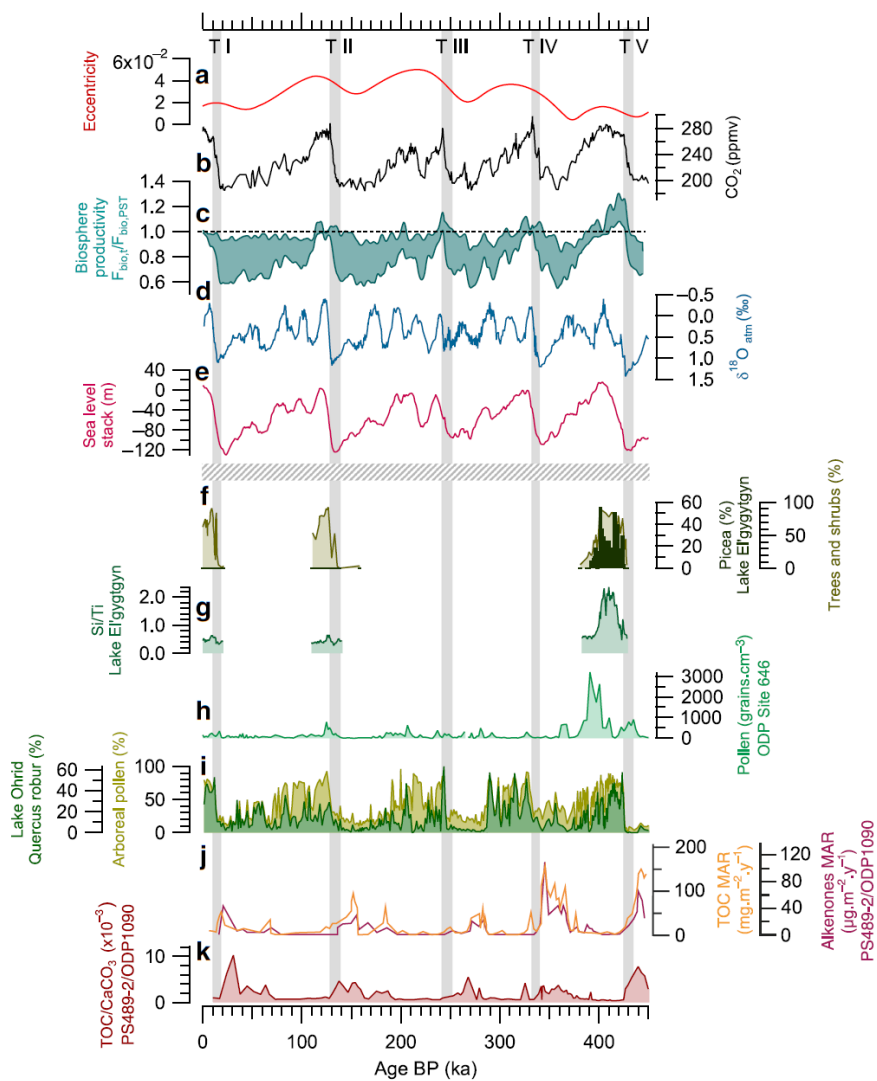


Figure 2. Global and regional productivity records since 450 ka. **a** Eccentricity. **b** CO<sub>2</sub> record (ppmv). **c** Reconstructed envelop for the ratio between global biosphere productivity and pre-industrial biosphere productivity as inferred from Δ<sup>17</sup>O of O<sub>2</sub> at age t (interpolation to 200 years and 101 binomial smoothing with Igor software). **d** δ<sup>18</sup>O<sub>atm</sub> record from the EDC ice core. **e** LR04 Sea level stack (m compared to present) on AICC2012 timescale. **f** Trees, shrubs and Picea pollen (%); **g** Si/Ti ratio; a proxy of biogenic silica normalised to detrital, reflecting the changes in diatom productivity in the lake. **h** Pollen abundance (grains.cm<sup>-3</sup>) of ODP Site 646. **i** Arboreal and Quercus robur pollen records (%) from Lake Ohrid, Balkan Peninsula. **j** Alkenone mass accumulation rate (MAR) (μg m<sup>-2</sup> year<sup>-1</sup>) and TOC MAR (mg·m<sup>-2</sup> year<sup>-1</sup>) records at Site PS2489-2/ODP1090. **k** TOC/CaCO<sub>3</sub> ratio at Site PS2489-2/ODP1090, Atlantic Southern Ocean. The horizontal dotted line separates the ice core records presented on the AICC2012 timescale (above the line) and the terrestrial and oceanic records presented on the age model of each core (under the line). The grey shadow bars represent the period of rapid increase in atmospheric CO<sub>2</sub>.

#### 4. 新的磁测资料显示南海在海底扩张过程中出现了连续的洋脊跃迁和旋转



翻译人：刘伟 [inewway@163.com](mailto:inewway@163.com)

*Qingsheng Guan, Tao Zhang et al. New magnetic data indicate successive ridge jumps and rotations of seafloor spreading in the South China Sea [J]. Earth and Space Science, 2020, doi.org/10.1002/essoar.10502989.1*

**摘要：**新的船载测量提供了一个覆盖南海东部次海盆(ESB)的高覆盖率磁异常数据集。海底扩张的磁异常是利用这一数据集来识别的，并结合了 IODP 349/367/368 航次的相关数据和年龄来进行约束。基于识别的磁异常，我们提出了一个高分辨率的 ESB 海洋地壳年龄模型。ESB 中的海底扩张开始于~ 30ma (C11n)，终止于~ 16ma (C5Br)。传播方向在 C6Cr 和 C5Er 之间呈逐渐的逆时针旋转，在 C5Dr 处呈明显的逆时针旋转。扩张旋转作用导致了扩张脊的分割和方向重置，形成了一系列 S 型断裂带。对磁异常的解释表明，在 C9r、C8n 和 C7n 发生了三个向南的洋脊跃迁，在 C5Dr 发生了一个同步跃迁。向南的三次脊跃使两翼之间的距离相差约 184 公里，并在今天的北翼留下了成对的磁异常条带 C10r-C7r。同步跃迁使扩张脊快速逆时针旋转，并与海底斜交。我们推测这些跃迁和旋转是海底扩张过程中的常见过程，是对南海周围的板块或微板块构造的动力学响应。

**ABSTRACT:** New shipborne surveys provide a closely spaced magnetic anomaly dataset covering the East Subbasin (ESB) of the South China Sea (SCS). Magnetic anomalies of seafloor spreading are identified using the dataset supplemented with previous data and age constraints from recent International Ocean Discovery Program Expeditions 349 and 367/368 holes. We present a high-resolution oceanic crustal age model and associated magnetic lineations of the ESB based on identified magnetic anomaly picks. Seafloor spreading in the ESB initiated at ~30 Ma (C11n) and terminated at ~16 Ma (C5Br). The spreading direction has experienced a gradual counterclockwise rotation between C6Cr and C5Er and a significant counterclockwise rotation at C5Dr. The spreading rotations reorganized the orientation and segmentation of the spreading ridge, resulting in the formation of a series of S-shaped fracture zones. The interpretation of the magnetic lineations reveals that three southward ridge jumps occurred at C9r, C8n, and C7n and a synchronous jump occurred at C5Dr. Three southward ridge jumps contributed to a total difference of ~184 km in the distance between the two flanks and left the paired magnetic lineations C10r-C7r on the present-day

north flank. The synchronous jump caused the spreading ridge to rotate rapidly counterclockwise and obliquely intersect the existing seafloor. We postulate that these ridge jumps and rotations are common processes during seafloor spreading reorientation and are dynamic responses to the plate or microplate tectonics around the SCS.

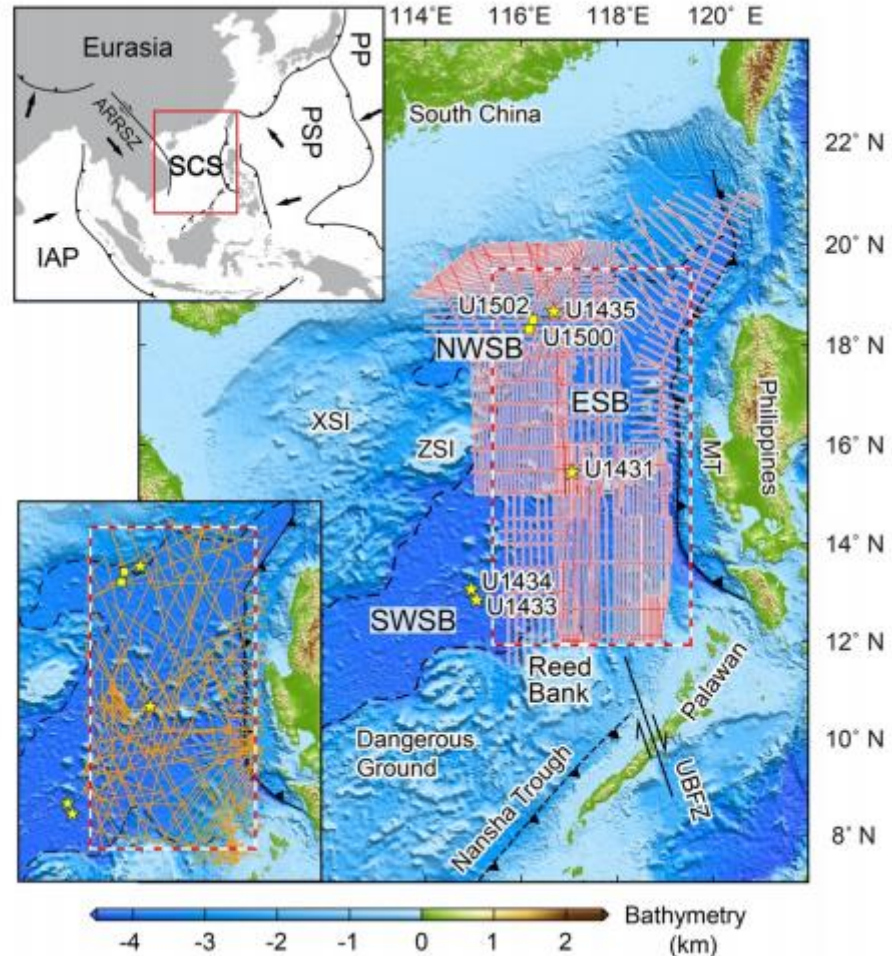


Figure 1. Location of the SCS and tracks of magnetic profiles. Red box marks the research area of this study. Red lines indicate sea surface magnetic tracks. Yellow stars indicate the drilling sites of IODP Expedition 349 (Li et al., 2015). Yellow squares indicate the drilling sites of IODP Expeditions 367 and 368 (Sun et al., 2018). Black dashed lines indicate the continent-ocean boundary determined from the vertical gravity gradient (Sandwell et al., 2014). The upper left inset shows the plate tectonic setting. The lower left inset shows supplementary magnetic tracks obtained from the National Centers for Environmental Information. XSI, Xisha Islands; ZSI, Zhongsha Islands; ARRSZ, Ailaoshan-Red River Shear Zone; MT, Manila Trench; UBFZ, Ulugan Bay Fault Zone; IAP, Indo-Australian Plate; PSP, Philippine Sea Plate; PP, Pacific Plate.

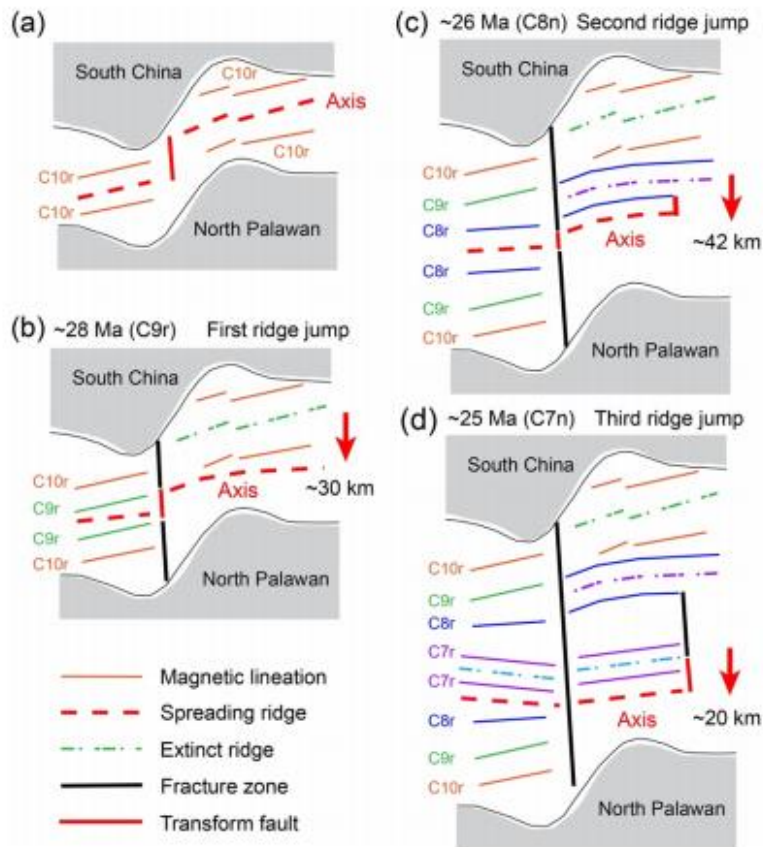


Figure 2. Schematic diagram of successive ridge jumps during the early spreading stage.

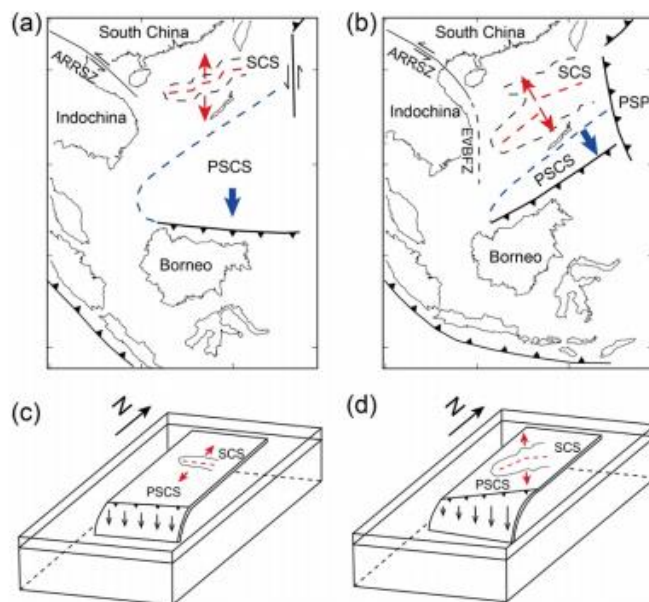


Figure 3. Structural sketch of the study area. (a) The PSCS subducted southward during the early spreading stage of the SCS. (b) The subduction direction of the PSCS gradually changed to the southeast, with the counterclockwise rotation of Borneo. (c) and (d) are schematic models of (a) and (b), respectively. ARRSZ, Ailaoshan-Red River Shear Zone. EVBFZ, East Vietnam Boundary Fault Zone. PSP, Philippine Sea Plate.

## 5. 海底磁化强度：低温氧化导致的钛磁铁矿颗粒的压力和结构变化



翻译人：李园洁 liyj3@sustech.edu.cn

Fabian K, Shcherbakov V P. *The magnetization of the ocean floor: Stress and fracturing of titanomagnetite particles by low-temperature oxidation*[J]. *Geophysical Journal International*, 2020, 221(3): 2104-2112.

**摘要：**海底的天然剩磁(NRM)主要由钛磁铁矿颗粒产生，其最初冷却成岩后经历低温氧化过程。这种氧化过程在大于  $5 \mu\text{m}$  的颗粒中产生收缩裂缝，这可能整个海底 NRM 强度的长波长变化的来源。本文，我们通过解决间隙扩散方程，开发一种量化的单相氧化和裂缝形成的理论，来描述球形钛磁铁矿颗粒的氧化过程，其扩散系数随着间隙增加大大降低。后一种的相关关系已经通过实验证明，对解释观测到的氧化程度随着海底年龄变化是非常重要的。计算得出的扩散曲线可提供氧化的钛磁铁矿球体内部的精确应力分布，并预测收缩裂缝的尺寸范围，与显微观测到的海底玄武岩样品的裂缝尺寸一致。新的扩散模型为过去已知的实验现象提供一些解释：(1) 实验室加热过程中低温氧化开始的温度  $200\text{--}400^\circ\text{C}$ ，取决于颗粒大小；(2) 需要加热到  $400\text{--}500^\circ\text{C}$  才能获得足够氧化  $z \approx 0.8$  形成高温固溶片晶。对海底条件的定量计算表明最初的  $40 \text{ ka}$  期间 NRM 强度快速降低，这是由于出现在具有亚临界尺寸的钛磁铁矿颗粒的强压和更大颗粒中形成裂缝的磁畴状态的随机性引起磁化强度偏转。

**ABSTRACT:** The natural remanent magnetization (NRM) of the ocean floor is carried by titanomagnetite grains that undergo low-temperature oxidation after initial cooling. Progressing oxidation is known to generate shrinkage cracks in grains larger than approximately  $5\mu\text{m}$ , and is suspected to control the long wavelength variation of NRM-intensity across the ocean floor. Here we develop a quantitative theory of single-phase oxidation and crack formation by solving the vacancy-diffusion equation that describes the oxidation process for spherical titanomagnetite particles, where the diffusion coefficient strongly decreases with vacancy concentration. The latter dependence has been experimentally demonstrated and is essential to explain the peculiarities of the observed variations of oxidation-degree with ocean-floor age. The calculated diffusion profiles provide the exact stress distributions inside oxidized titanomagnetite spheres, and predict a size limit for shrinkage-crack formation that agrees with microscopic observations of crack appearance in ocean-floor basalt samples. The new diffusion model provides a unified explanation of long-known experimental facts that (1) temperatures for the onset of low-temperature oxidation during laboratory heating are theoretically estimated as  $200\text{--}400^\circ\text{C}$ , depending on grain size and (2) that

heating to 400–500 °C is required to obtain a sufficiently high degree of oxidation  $z \approx 0.8$  for the development of high-temperature exsolution lamellae. Calculations for ocean-floor conditions quantitatively suggest that a rapid decrease of NRM intensity during the first 40 ka results from a deflection of magnetization by strong stresses that emerge in titanomagnetite grains of subcritical sizes, and randomization of domain-state by crack formation in larger grains.

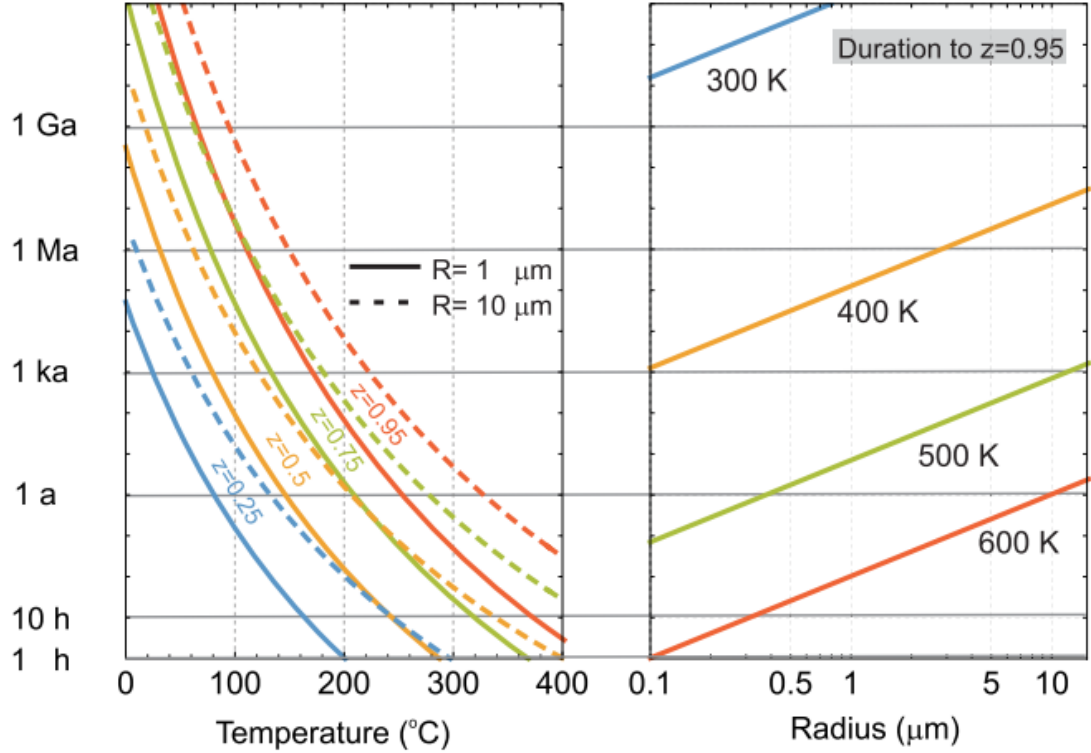


Figure 1. Left-hand panel: model results for the duration to central oxidation states  $z = 0.25, 0.5, 0.75, 0.95$  for spherical TM particles of radius  $R = 1 \mu\text{m}$  (solid lines) and  $R = 10 \mu\text{m}$  (dashed) as function of temperature. Right-hand panel: duration to central oxidation state  $z = 0.95$  for spherical TM particles at temperatures  $T = 300, 400, 500, 600 \text{ K}$  as function of particle radius. Calculations use  $\mu = 9500 \text{ kB K}$ , and  $E_0 = 10500 \text{ kB K}$ .

6. 根据新的重力(EIGEN 6C4)及其他方面数据确定在西伯利亚(Popigai)附近的一个 200km 疑似陨石坑 Kotuykanskaya



翻译人：曹伟 11930854@mail.sustech.edu.cn

*Jaroslav Klokoník, Kosteleck J, Ale Bezděk, et al. A 200 km suspected impact crater Kotuykanskaya near Popigai, Siberia, in the light of new gravity aspects from EIGEN 6C4, and other data[J]. Scientific Reports, 2020, 10(1):6093*

**摘要：**我们提供的论据有助于确定俄罗斯西伯利亚(Popigai)附近一个 200 公里的疑似陨石坑 Kotuykanskaya。我们使用的重力方面数据包括重力扰动，扰动位势二阶导数的 Marussi 张量，重力不变量及其比值，走向角度以及虚拟变形，这些数据全部来源于组合静态重力场模型 EIGEN 6C4，该模型地面分辨率约 10 km，精度约 10 milliGals。同时我们还使用了来自 EMAG2 模型中的磁异常，强调了可疑区域的深部场源证据，从而约束了该构造的影响来源。

**ABSTRACT:** We provide arguments in favour of impact origin of a 200 km suspected impact crater Kotuykanskaya near Popigai, Siberia, Russia. We use the gravity aspects (gravity disturbances, the Marussi tensor of the second derivatives of the disturbing geopotential, the gravity invariants and their specific ratio, the strike angles and the virtual deformations), all derived from the combined static gravity field model EIGEN 6C4, with the ground resolution of about 10 km and a precision of about 10 milliGals. We also use the magnetic anomalies from the model EMAG2 and emphasize the evidence of much deeper sources in the suspected area, constraining the impact origin of this structure.

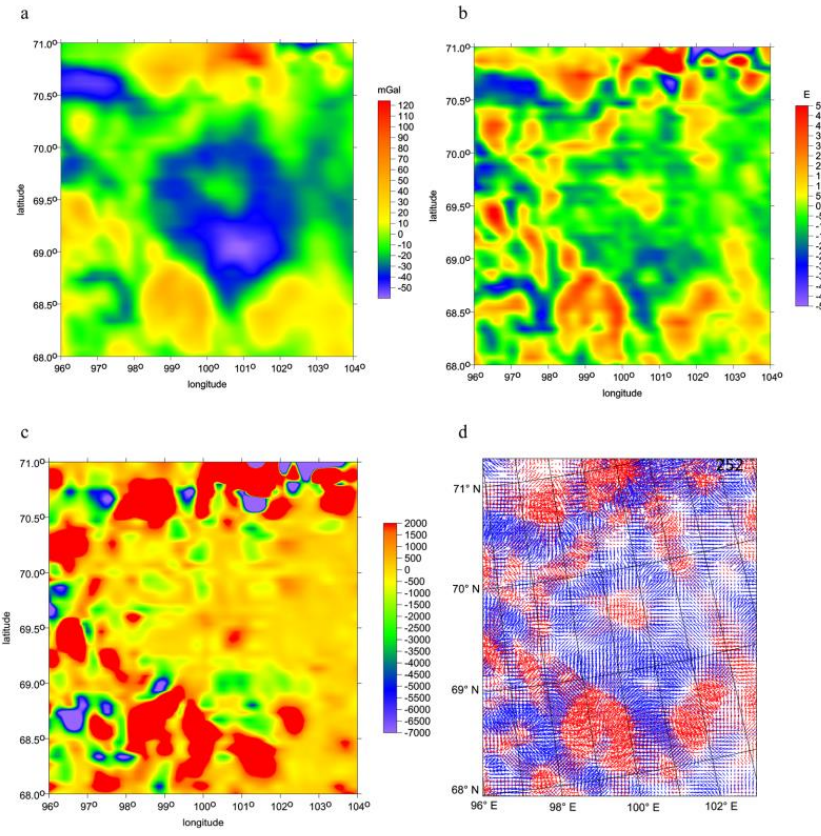


Figure 1. The gravity disturbances  $\Delta g$  [mGal], the radial second order derivative  $T_{zz}$  [E], the gravity invariant  $I_2$  [ $s^{-6}$ ], and the virtual deformations  $v_d$  [-] (red for dilatation, blue for compression) in the Kotuykanskaya II suspected impact crater, computed with EIGEN 6C4. Owing to high latitude, to get reliably plotted orientation of  $v_d$  “vectors”, we had to use for this gravity aspect the polar projection.

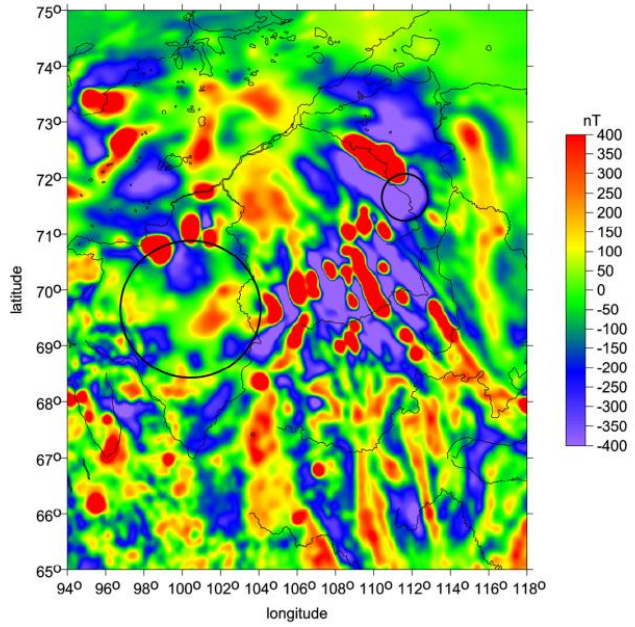


Figure 2. Magnetic anomalies [nT] for the Popigai and Kotuykanskaya area according to EMAG2. Note that the magnetic anomalies have sharp contrast and larger magnitudes outside the suspected crater boundary while inside the crater boundary, anomalies have smaller magnitudes and are blurred.

## 7. 葫芦洞石笋记录的末次冰期大气 $^{14}\text{C}/^{12}\text{C}$ 变化

翻译人：郑威 11930589@mail.sustech.edu.cn



Cheng H, Edwards R L, Southon J, et al. Atmospheric  $^{14}\text{C}/^{12}\text{C}$  changes during the last glacial period from Hulu Cave[J]. *Science*, 2018, 362(6420): 1293-1297.

**摘要：**成对测量的两个葫芦洞石笋的 $^{14}\text{C}/^{12}\text{C}$ 和 $^{230}\text{Th}$ 年龄完善了全部 $^{14}\text{C}$ 定年范围（约54,000年）的大气 $^{14}\text{C}$ 记录。在末次冰期，大气 $^{14}\text{C}/^{12}\text{C}$ 范围从近似现今值到比现今值高1.70倍不等（42,000-39,000年前）。后者对应的 $^{14}\text{C}$ 年龄比标准年龄少了5200年，并且与Laschamp地磁极偏移以及随后的H4事件相关。千年尺度的变化很大程度上归因于地磁场的变化以及部分归因于海洋碳循环中与气候相关的变化。在25,000到11,000年前逐步降低的 $^{14}\text{C}/^{12}\text{C}$ 值可能在某种程度上与逐步增强的海洋通气速率有关。

**ABSTRACT:** Paired measurements of  $^{14}\text{C}/^{12}\text{C}$  and  $^{230}\text{Th}$  ages from two Hulu Cave stalagmites complete a precise record of atmospheric  $^{14}\text{C}$  covering the full range of the  $^{14}\text{C}$  dating method (~54,000 years). Over the last glacial period, atmospheric  $^{14}\text{C}/^{12}\text{C}$  ranges from values similar to modern values to values 1.70 times higher (42,000 to 39,000 years ago). The latter correspond to  $^{14}\text{C}$  ages 5200 years less than calibrated ages and correlate with the Laschamp geomagnetic excursion followed by Heinrich Stadial 4. Millennial-scale variations are largely attributable to Earth's magnetic field changes and in part to climate-related changes in the oceanic carbon cycle. A progressive shift to lower  $^{14}\text{C}/^{12}\text{C}$  values between 25,000 and 11,000 years ago is likely related, in part, to progressively increasing ocean ventilation rates.

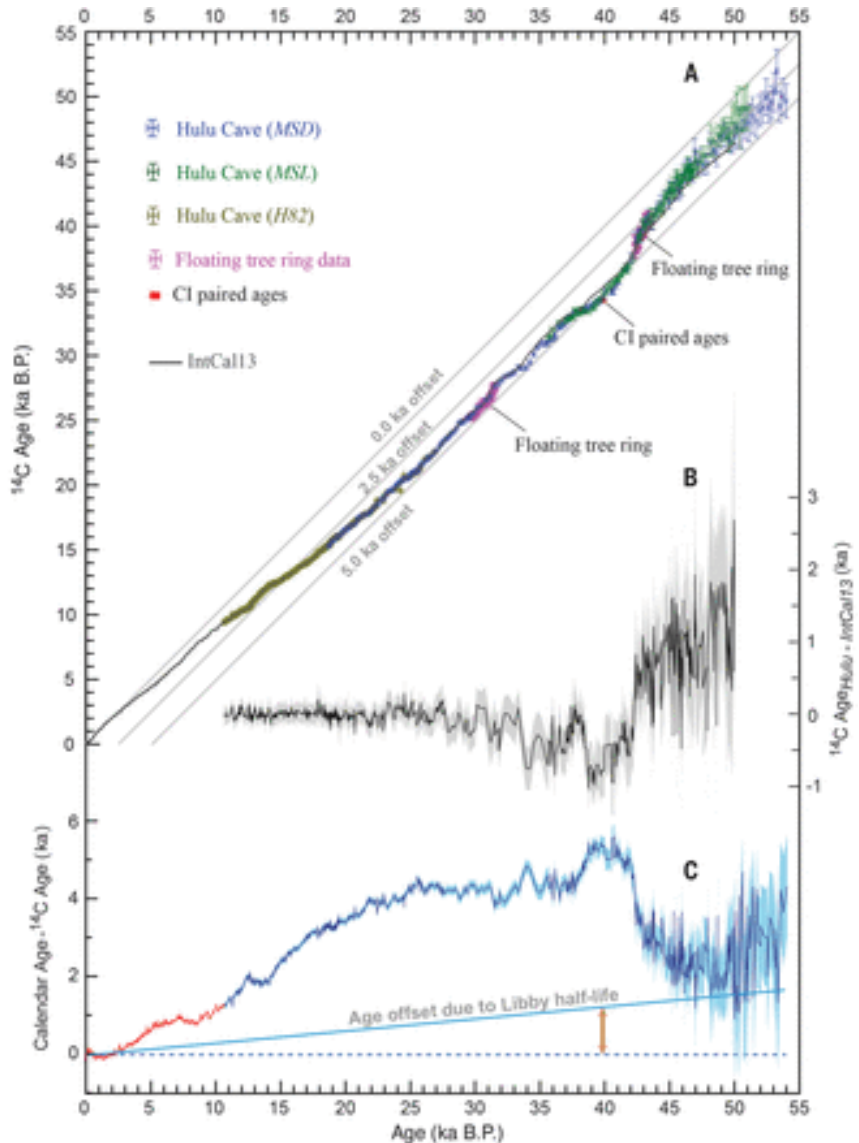


Figure 1. Hulu speleothem  $^{14}\text{C}$  versus  $^{230}\text{Th}$  ages and comparison between Hulu and IntCal13  $^{14}\text{C}$  ages. (A) Hulu [olive-brown, H82 (8); blue, MSD, and green, MSL (this study), and IntCal13  $^{14}\text{C}$  (17)] vs.  $^{230}\text{Th}$  ages.  $^{14}\text{C}$  error bars are  $1\sigma$ . For clarity, uncertainties in IntCal13 are not shown. The floating tree ring  $\Delta^{14}\text{C}$  datasets (purple) (14, 15) are tuned to the Hulu  $^{14}\text{C}$  record (11). The red square ( $1\sigma$ ) is the independent data point based on  $^{14}\text{C}$  measurements on wood associated with the Ar-Ar dated Campanian Ignimbrite (13). (B)  $^{14}\text{C}$  age difference (black) between Hulu dataset and IntCal13 (17). The gray envelope shows the uncertainty ( $1\sigma$ ). Hulu  $^{14}\text{C}$  ages are corrected for the DCF ( $450 \pm 70$  years) (8). (C) Calendar age minus IntCal13 (red)/Hulu (blue)  $^{14}\text{C}$  age. The light blue envelope shows the uncertainty ( $1\sigma$ ). The three Hulu sample datasets replicate over contemporary growth periods. Hulu Cave  $^{14}\text{C}$  data are consistent with IntCal13 between  $\sim 10.6$  and  $33.3$  ka B.P. but lower in  $^{14}\text{C}$  ages between  $\sim 33.3$  and  $42$  ka B.P. and higher between  $42$  and  $53$  ka B.P.

## 8. 南海中新世晚期 *Tridacnidae* 碳同位素变化的控制机制



翻译人：王浩森 502691781@qq.com

Yang Z, Shao D, Mei Y, et al. 2019. *The controlling mechanism of mid- to late Holocene carbon isotopic variations of Tridacnidae in the South China Sea*. *Marine Geology* [J], 415: 105958.

**摘要：**生物碳酸盐中的碳同位素分馏过程非常复杂，生物碳酸盐  $\delta^{13}\text{C}$  的季节性和长期变化机制仍存在争议。在本研究中，从南海收集了 5 个 *Tridacnidae* 样本，并进行了详细分析以研究季节变化。高分辨率的  $\delta^{13}\text{C}$  记录表现出周期性变化，这可能与环境参数（例如 Chl-a 浓度，盐度，SST，降雨）的季节性变化有关。收集并分析了 57 个 *Tridacnidae*，以研究全新世中晚期 *Tridacnidae*- $\delta^{13}\text{C}$  的千年尺度变化及其控制机理。在一定的统计意义上，在 500-5500 BP 期间，*Tridacnidae* 的  $\delta^{13}\text{C}$  与太阳活动（TSI 和黑子数）显着相关，这很可能是由于 *Tridacnidae* 存在共生虫黄藻。太阳活动可能会显着影响其代谢活性，并影响 *Tridacnidae* 的微环境，进而影响 *Tridacnidae* 的  $\delta^{13}\text{C}$  组成。在过去的 200 多年里，*Tridacnidae*- $\delta^{13}\text{C}$  与太阳活动之间的关联性下降很可能是由于人为产生的 CO<sub>2</sub> 的增加和海洋  $\delta^{13}\text{C}$ -Suess 效应所致。这项研究提高了我们对 *Tridacnidae* 中  $\delta^{13}\text{C}$  的季节性和长期变化的认识。

**ABSTRACT:** The carbon isotopic fractionation process in biogenic carbonate is very complex, and the mechanism for seasonal and long-term variations in biogenic carbonate  $\delta^{13}\text{C}$  remains a matter of debate. In this study, 5 *Tridacnidae* samples were collected from the South China Sea and analyzed in detail to study seasonal variations. The high-resolution  $\delta^{13}\text{C}$  records exhibited cyclic variations, likely related to seasonality in environmental parameters (e.g., Chl-a concentration, salinity, SST, rainfall). 57 *Tridacnidae* were collected and analyzed to study the millennium-scale changes of *Tridacnidae*  $\delta^{13}\text{C}$  during the mid- to late Holocene and the controlling mechanism. The *Tridacnidae*  $\delta^{13}\text{C}$  over the period 500–5500 BP is statistically significantly correlated with solar activity (TSI and sunspot number), likely attributed to the presence of symbiotic zooxanthellae within *Tridacnidae*'s mantle lobes. Solar activity could significantly affect the metabolic activity of zooxanthellae, *Tridacnidae*'s microenvironment, and thus *Tridacnidae*'s  $\delta^{13}\text{C}$  composition. The decoupling between the *Tridacnidae*  $\delta^{13}\text{C}$  and solar activity over the past 200 years is most likely due to increased amount of anthropogenic CO<sub>2</sub> and the oceanic  $\delta^{13}\text{C}$  Suess effect. This study improves our understanding about the seasonal and long-term variations of  $\delta^{13}\text{C}$  in *Tridacnidae*.

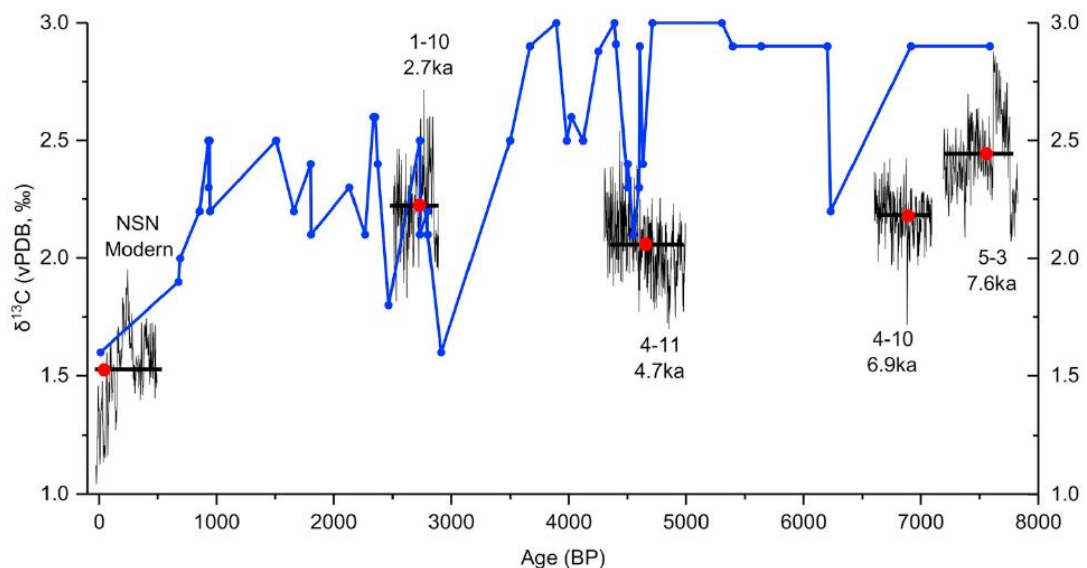


Figure 1. Temporal variations of *Tridacnidae*  $\delta^{13}\text{C}$  over the past 7600 years. The blue line represents the  $\delta^{13}\text{C}$  values of the individual *Tridacnidae*, and black line the detailed  $\delta^{13}\text{C}$  values of five representative *Tridacnidae*. Black horizontal lines indicate the average *Tridacnidae*  $\delta^{13}\text{C}$  for different periods, and the red dots represent the exact age and average  $\delta^{13}\text{C}$  values of the five representative *Tridacnidae*. (For interpretation of the references to colour in this figure legend, the reader is referred to the web version of this article.)

## 9. 温度和海水同位素组成对日本沿海两根 83ka 以来的石笋记录的控制



翻译人：杨会会 11849590@mail.sustech.edu.cn

Taiki M, Kenji K, Shota A et al. *Temperature and seawater isotopic controls on two stalagmite records since 83 ka from maritime Japan* [J]. *Quaternary Science Reviews*, 2018, 192: 47-58

**摘要：**末次盛冰期（LGM）时期的千年尺度暖阶的 D-O 旋回和寒阶的 H 事件具有明显的古气候特征。D-O 和 H 事件在北大西洋区首次被证实。这些暖阶的和冷阶的事件在世界其他地方的海洋和陆地高分辨率记录中都有表现，但是区域气候变化的幅度和模式仍然没有得到很好的量化。本文中我们展示了来自日本中部的两个重复石笋的  $\delta^{18}\text{O}$  记录，他们的年代可以追溯到 83.4 ka。这两根石笋清楚地记录了 H7 到 H3 事件，但没有记录到 D-O 循环。这两个日本石笋的一个重要特征是全新世中期与末次盛冰期的  $\delta^{18}\text{O}$  值相差较小(约 2.9‰)。更靠近海区的那根石笋，其  $\delta^{18}\text{O}$  值的长期趋势一般遵循海水  $\delta^{18}\text{O}$  记录，占全新世中期与末次盛冰期差异的约 1.1‰~2.9‰。剩下的 1.8‰ 的差异可以由 LGM 到中全新世的 9°C 升温及 H 事件期间 3°C 的降温来解释，这与前人估算的日本岛陆地的古温度可以比较。衰减的同位素信号与暖阶的 D-O 旋回相关联，指示大西洋的暖化信号并没有传到日本海域。这些日本石笋的同位素记录特征，是由于其地理位置处于温湿的黑潮暖流附近。

**ABSTRACT:** Millennial-scale interstadial Dansgaard-Oeschger (D-O) cycles and Heinrich (H) stadial events are pronounced paleoclimatic features during the last glacial period, which were first demonstrated in the North Atlantic region. These stadial and interstadial events are expressed in marine and terrestrial high resolution records elsewhere in the world, but the magnitude and mode of the regional climate changes are still poorly quantified. Here we present new replicated stalagmite  $\delta^{18}\text{O}$  profiles from two caves in central Japan, which extend back to 83.4 ka. The records clearly display the H7 to H3 events, but not D-O cycles. An important feature of the two Japanese stalagmites is the small difference (~2.9‰) in  $\delta^{18}\text{O}$  values between the mid-Holocene and the Last Glacial Maximum (LGM). Long-term trends of the stalagmite  $\delta^{18}\text{O}$  values at the more maritime site generally follow that of the  $\delta^{18}\text{O}$  record of seawater, which is responsible for ~1.1‰ of the ~2.9‰ difference between mid-Holocene and LGM. The remaining 1.8‰ in the difference can be accounted for by + 9°C of warming between the LGM and mid-Holocene and -3°C cooling at H events, which are comparable with the previous estimates of land paleotemperature in the Japanese

Islands. The attenuated isotopic signal associated with D-O interstadials indicates that the warming in the Atlantic did not significantly transfer to the maritime Japan. These unique features of the isotopic records of the Japanese stalagmites are due to the geographic position at the vicinity of the moisture source, Kuroshio warm current.

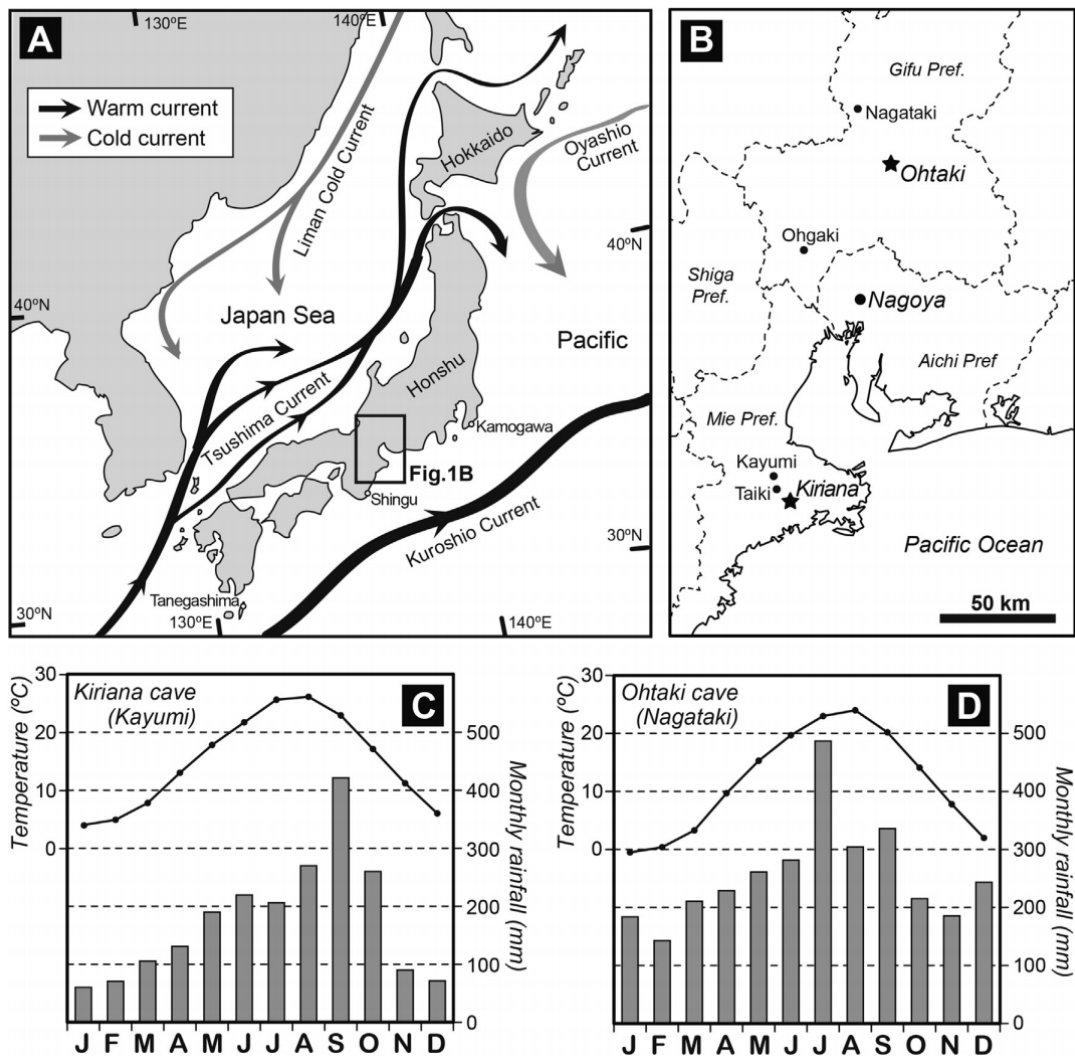


Figure 1. Geographic and climate conditions of the study localities, Kiriana and Ohtaki caves. A) Map of the Japanese Islands showing localities cited in this study. Major routes of Kuroshio and other currents are also shown. B) Map of central Japan showing the locations of the caves (Kiriana and Ohtaki) and sampling points of rainwater (Taiki and Ohgaki). C) Monthly average (2000-2014) temperature and rainfall at Kayumi observatory. D) Monthly average (2000-2014) temperature and rainfall at Nagataki observatory.

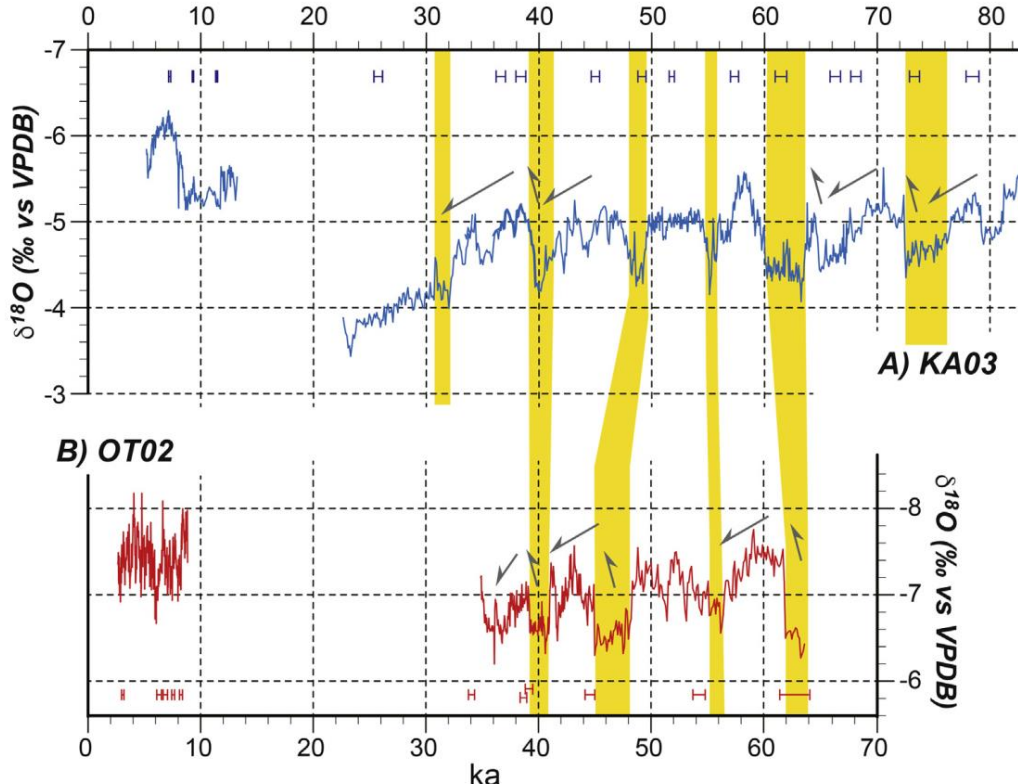


Figure 2.  $\delta^{18}\text{O}$  (VPDB) profiles of two stalagmites, KA03 (A) and OT02 (B).  $\delta^{18}\text{O}$  values of the stalagmite OT02 vary in a range from  $-8.2\text{\textperthousand}$  to  $-6.3\text{\textperthousand}$  (Fig. 3B; Table S1). OT02 record displays a similar overall pattern to KA03, except that values are offset to lower values by about  $-2.5\text{\textperthousand}$  compared to KA03. At 34.8-63.5 ka, this  $\delta^{18}\text{O}$  record is punctuated with four millennial-scale events with increases in  $\delta^{18}\text{O}$  values of 0.5-1‰ (yellow bars in Fig. 3B). These four events are temporally well correlated with the events recognized in KA03, except for one at 45-48 ka. The chronological discrepancy of this event (48-50 ka in KA03 and 45-48 ka in OT02) is most likely due to age uncertainties of the interval (around  $\pm 1.0$  kyr in KA03 and  $\pm 1.6$  kyr in OT02). A saw toothed appearance can be recognized but is less clear than KA03. Instead, several short-lived intervals with lower  $\delta^{18}\text{O}$  values occur 54-41 ka, which are not distinct in KA03. The  $\delta^{18}\text{O}$  values of the upper Holocene portion (9-3 ka) of the record mostly fall between  $-7$  and  $-8\text{\textperthousand}$  (Fig. 3B). (For interpretation of the references to color in this figure legend, the reader is referred to the Web version of this article.)